

Accelerator Physics

Reported by David Robin

In 1998 the ALS user community experienced a substantial improvement in the quality and consistency of the delivered beam. In particular, both fast and slow electron beam motions were significantly reduced. With the implementation of a “slow” global orbit feedback system, the horizontal orbit drift was reduced by a factor of 5, from ± 50 microns peak-to-peak to less than ± 10 microns peak-to-peak. By replacing the rf master oscillator with a quieter version, the orbit noise at 4 kHz was reduced by a factor of 6. These and other improvements were partly a result of close cooperation between the accelerator physics group and the users.

In addition to orbit stability, large gains were made in the understanding of lifetime and injection. One discovery was that the lifetime (which is determined primarily by intrabeam scattering) is limited by the dynamic aperture, not by the momentum acceptance defined by the rf system. By understanding this unexpected result it may be possible to improve the beam lifetime and to accurately predict it under new running conditions (such as with the superbends). Improvements were made in the understanding of injection dynamics. Using several diagnostics (streak camera, longitudinal feedback buttons) measurements were made of the phase and energy mismatch of the injected beam relative to the stored beam. These and other studies of the injection dynamics should lead to higher and more stable injection rates. This will be particularly important if the machine is to be run in a top-off mode, refilled every 12 hours instead of every 4.

During 1998 the elliptically polarized undulator (EPU) was installed in the machine. Unlike other insertion devices whose gaps only move vertically to change the photon energy, the EPU's gap also shifts longitudinally to change the polarization. It was not clear if the orbit motion generated by this extra degree of gap motion could be compensated for in the same manner as is done in the other devices—with feedforward tables. Studies showed that it was possible and practical to generate and operate with a 2-D feedforward table for orbit compensation. At this point the longitudinal motion is limited to 1/10th of its maximum speed. The challenge remains to compensate the orbit when the “speed limit” is lifted.

To increase the beam lifetime, a third-harmonic cavity system will be installed in the storage ring in the June 1999 shutdown. Construction of the third-harmonic cavities is nearly complete, and commissioning of the system will take place during summer 1999. In addition, plans are underway to install three high-field (5-T) superconducting bend magnets in the storage ring. These “superbends” will be excellent sources of x rays. The plan is to install them in 2001. Theoretical accelerator physics studies of the superbends indicate that there will be no significant detriment to the performance of the machine.

Orbit Stability in the 0-300 Hz Region

Reported by Greg Portmann

The third-generation Advanced Light Source produces extremely bright and finely focused photon beams using undulators, wigglers, and bend magnets. The dominant causes of orbit motion at the ALS are temperature variation and insertion device motion. This type of motion can be removed using slow global orbit feedback with a data rate of a few hertz. The remaining orbit motion up to 300 Hz is only 1-3 micron rms. Since slow orbit feedback does not require high computational throughput, the global orbit feedback algorithm, based on the singular valued decomposition method, is coded in MATLAB and runs on a control room workstation. Using the

MATLAB environment to develop, test, and run the storage ring control algorithms has proved to be a fast and efficient way to operate the ALS.

Orbit Stability and Feedback

Maintaining the proper electron beam orbit is an important operational issue for all light sources. The most commonly used figure of merit for orbit stability is that the beam should be stable to one-tenth of the beam size. Expressed another way, the optics for most light source experiments can tolerate a ten percent fluctuation in the beam's position and angular divergence without adverse effects. As shown in Table 1, this implies a very tight tolerance for orbit motion at the ALS source points (table calculated assuming 1.8% coupling).¹

Table 1. Beam position stability requirements.

Beam Location	Horizontal	Vertical
Straight Section	24.6 μm	2.0 μm
Bend Magnet #1	5.3 μm	4.4 μm
Bend Magnet #2	10.3 μm	1.2 μm

Local and global orbit feedback algorithms can potentially regulate the beam position to the accuracy of the beam position monitor (BPM) system; however, building a BPM system that is accurate to the micron level is quite difficult. Many third-generation light sources have BPM systems capable of submicron accuracy over relatively short time intervals. At the ALS, the electron beam can be accurately measured to 0.6 μm horizontally and 0.8 μm vertically over a 0.1–300 Hz frequency range. The problem for measuring beam motion at the ALS is over longer time intervals. The two major sources of error are the current dependence of the BPM electronics and physical motion of the vacuum chamber. (Harmonic correction algorithms can be used to mitigate these effects.) Due to these problems, we have taken a very conservative approach to adding orbit feedback to the ALS storage ring.

In addition to the original 96 BPMs in the ALS storage ring, a pair of high-sensitivity BPMs have been installed in each insertion device straight section (20 BPMs total).² By rigidly mounting these BPMs to each insertion device structure that is installed in a temperature controlled housing, the positional stability of the BPM is ensured. The relative motion between the BPM and the storage ring floor is a few microns per week.³ With the addition of these new monitors, global orbit feedback in the horizontal plane has been added to the standard operation of the ALS.

Without orbit feedback, but with temperature stabilization of the tunnel-air and low-conductivity water, we have achieved the positional stability shown in Table 2.

¹ D. Robin, private communication (1998).

² J. Hinkson, private communication (1999).

³ G. Krebs, "Measurement of Storage Ring Motion at the ALS," *Proceedings of the 1997 IEEE Particle Accelerator Conf.*

Table 2. Beam stability without orbit feedback.

Frequency	Magnitude	Dominant Cause
Two weeks (A typical experimental run)	Horizontally $\pm 200 \mu\text{m}$ Vertically $\pm 100 \mu\text{m}$	Magnet hysteresis Temperature fluctuations Component heating between 1.5 GeV and 1.9 GeV
1 Day	Horizontally $\pm 125 \mu\text{m}$ Vertically $\pm 75 \mu\text{m}$	Temperature fluctuations
4 Hour Fill	Horizontally $\pm 50 \mu\text{m}$ Vertically $\pm 20 \mu\text{m}$	Temperature fluctuations Feed forward errors
Minutes	5 to 10 μm	Feed forward errors
0.1 to 300 Hz	1 to 3 μm	Ground vibration

Slow Orbit Drift

The dominant source of orbit motion at the ALS is slow drift due to temperature variations. There are three basic causes of thermal variations: (1) change in ambient air temperature of the storage ring tunnel; (2) change in the low conductivity cooling water (LCW) temperature; and (3) change in the photon beam power as the electron beam decays. The regulation specifications are ± 0.2 and $\pm 0.1^\circ \text{C}$ for the air and LCW temperatures, respectively. However, temperature regulation to this level is difficult to achieve day-to-day.

Insertion device motion is the next largest source of slow orbit distortion. The ALS experimenters can freely adjust the insertion device gap at any time. Feedforward tables are empirically generated to compensate for this motion. The table accuracy is 5-10 μm rms.

Figures 1 and 2 show the electron beam orbit in the insertion device straight sections for a typical day before the orbit feedback system was operational. The horizontal orbit is more sensitive to temperature variation.

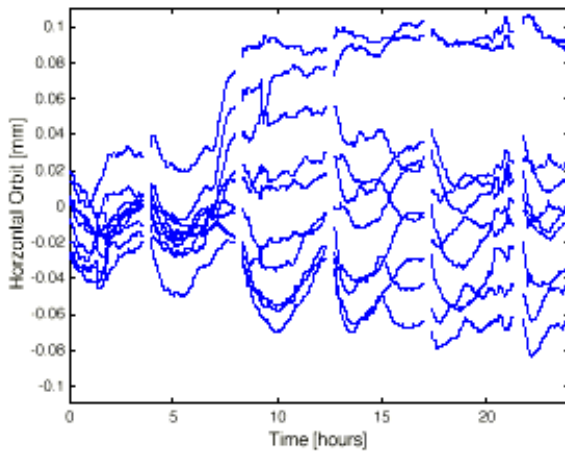


Figure 1. Horizontal orbit stability without feedback, August 15, 1998.

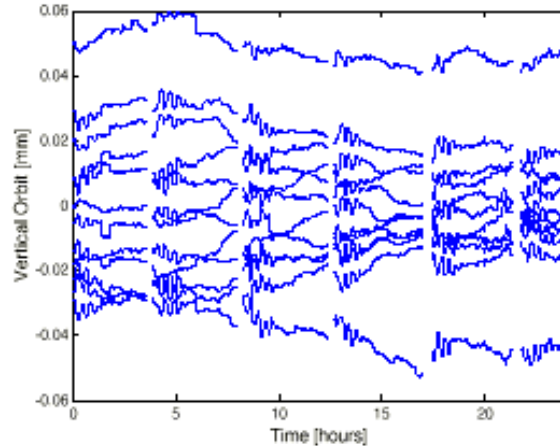


Figure 2. Vertical orbit stability without feedback, August 15, 1998.

A slow global orbit feedback system in the horizontal plane has been in operation at the ALS since September 1998. Before that time, orbit correction was only done at the beginning of an experiment run. Besides the feedforward correction to compensate for insertion device motion, the storage ring magnet control would be static for the length of the run—typically two weeks. As shown in Table 2, the ALS is surprisingly quite stable without orbit correction. However, in order to meet the tolerances in Table 1, a slow global orbit feedback system was developed. Figure 3 shows the results of applying the correction.

One could correct the orbit to the micron level, but the orbit correction algorithm is presently over-constrained. This is a conservative way of running, done so that the feedback system does not particularly track vacuum chamber motion.

“Fast” Orbit Motion

The dominant cause of “fast” orbit motion (up to about 300 Hz) at the ALS is vibration. Power supply regulation is a common cause of orbit stability problems in this frequency range; however, it thankfully has not been an issue at the ALS. Figure 4 shows the power spectrum for the orbit motion in the horizontal plane from 0.3–50 Hz. The rms motion from 0.1–300 Hz is typically 3.0 μm horizontally and 1.2 μm vertically. These numbers have not changed very much over the last five years, which implies that the ALS can inherently meet the stability goals (Table 1) in this frequency range without orbit feedback.

Future Work

Improving the orbit stability at the ALS will be a continual process. The immediate goal is to include vertical orbit correction with the slow orbit feedback and add faster orbit correction during insertion device gap motion. Once this is accomplished, the orbit stability goal given in Table 1 will be reliably achieved. Presently we achieve the stability goal by temperature regulation and maintaining accurate insertion device feed forward tables. This will continue to be important; however, with additional feedback, the reliability of orbit stability at the ALS will improve even further.

Presently, our knowledge of electron beam motion comes mainly from 20 electron beam position monitors (BPMs). Increasing the number of monitors and adding photon beam position monitors with adequate stability and bandwidth will be very helpful in diagnosing beam stability problems.

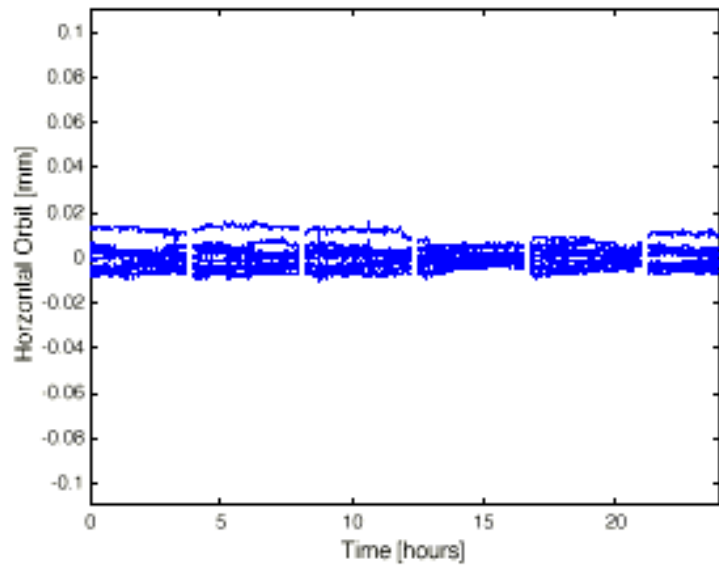


Figure 3. Horizontal orbit stability with feedback on, February 6, 1999.

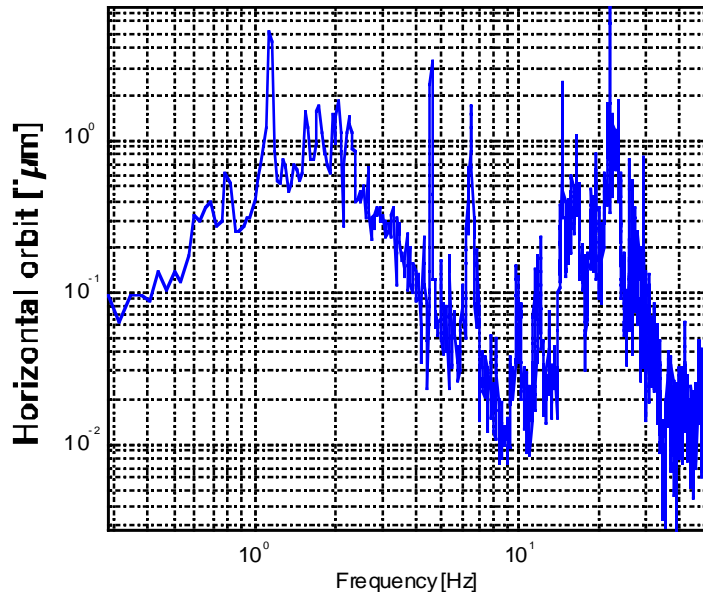


Figure 4. Power spectral density of the horizontal orbit.

Orbit Stability in the >300 Hz Region

Reported by John Byrd

Fast beam motion has several deleterious effects on photon beam quality. Synchrotron (longitudinal) electron beam motion results in increased average energy spread, which widens undulator harmonics, as well as increased horizontal beam size at dispersive lattice points, thereby reducing the beam brightness at these locations. Longitudinal motion can also result in erratic variation of centroid position and angle at dispersive lattice locations. Betatron, or transverse, motion can cause an average increase in the transverse beam size, also reducing the brightness. It also can result in erratic centroid motion or angle, leading to motion on the user's sample or intensity modulation through an aperture. Another possible result is erratic change in beam size, leading to intensity modulation through an aperture such as a slit.

There are several potential sources of fast beam motion at the ALS that either excite the beam directly or make possible self-excited beam motions (i.e., instabilities.) Sources driving the beam include random amplitude or phase noise in the rf system, exciting synchrotron oscillations; klystron power supply noise; and noise in the multibunch feedback systems. The sources of multibunch self-excited motion include rf cavity higher-order modes, resistive wall impedance (longitudinal and transverse), and vertical coupled bunch instabilities driven by ion trapping. In high-current single-bunch mode (i.e., above 4–5 mA/bunch), there are longitudinal microwave instabilities and a vertical mode-coupling instability, both driven by the broadband impedance of the vacuum aperture.

We have made several improvements in the area of fast beam motion over the past year. The main efforts have been in increasing the reliability of the multibunch feedback systems, both through hardware upgrades and operational adjustment. These efforts have been extremely successful, such that these systems operate almost without fail. Another area in which we made an improvement was in the understanding of how phase noise in the rf master oscillator excites synchrotron oscillations. This is described in more detail below.

Beam Motion Driven by RF Phase Noise

In the spring of 1998, scientists using the ALS infrared synchrotron light beamline (Beamline 1.4) reported observations of beam motion in the frequency range of 4 to 10 kHz, variable with total beam current. Our investigations linked the beam motion to energy oscillations of the beam at a point of dispersion in the lattice. These oscillations were found to be driven by phase noise in the rf master oscillator (MO) through the Robinson effect.

This effect, first explained by Robinson in 1964, describes the dynamics of the interaction between synchrotron oscillations of the beam and the fundamental mode of the rf cavity. Under normal cavity conditions, this interaction causes a damping of the beam's synchrotron oscillations as well as a downward shift in the oscillation frequency, illustrated in Figure 5, which shows the transfer function for beam energy oscillations excited by rf cavity phase modulation.

Although the beam-cavity interaction is inherently stable, beam oscillations can still be driven by modulations in the rf cavity amplitude or phase. One of the sources of excitation is phase noise on the rf master oscillator. The characteristic spectrum of phase noise decreases exponentially with distance from the carrier, as shown by the two spectra shown in Figure 5. The main problem is that the overlap of the beam response and the phase noise increases as the beam frequency is shifted to lower values at higher currents. Shown in Figure 6 are measured beam spectra at various beam currents along with a calculation of the expected beam motion using the known phase noise in the master oscillator. The agreement is good, enabling us to predict the beam motion for any noise source.

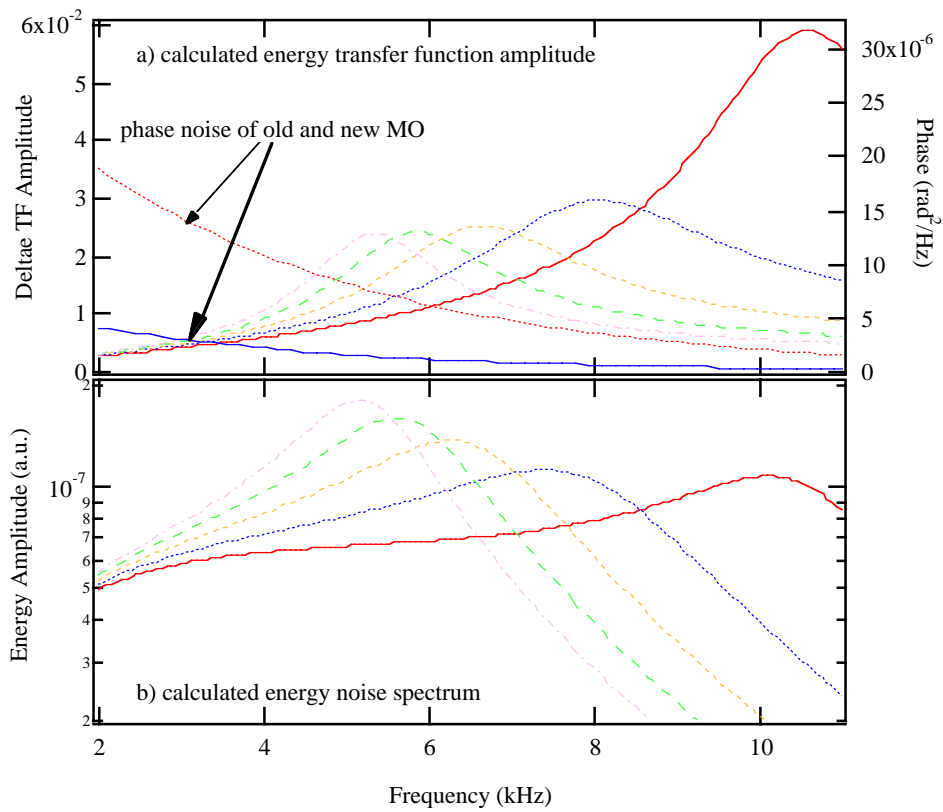


Figure 5. Beam energy transfer function as a function of beam current showing the Robinson frequency shift. The phase noise of two master oscillator (MO) sources is also shown.

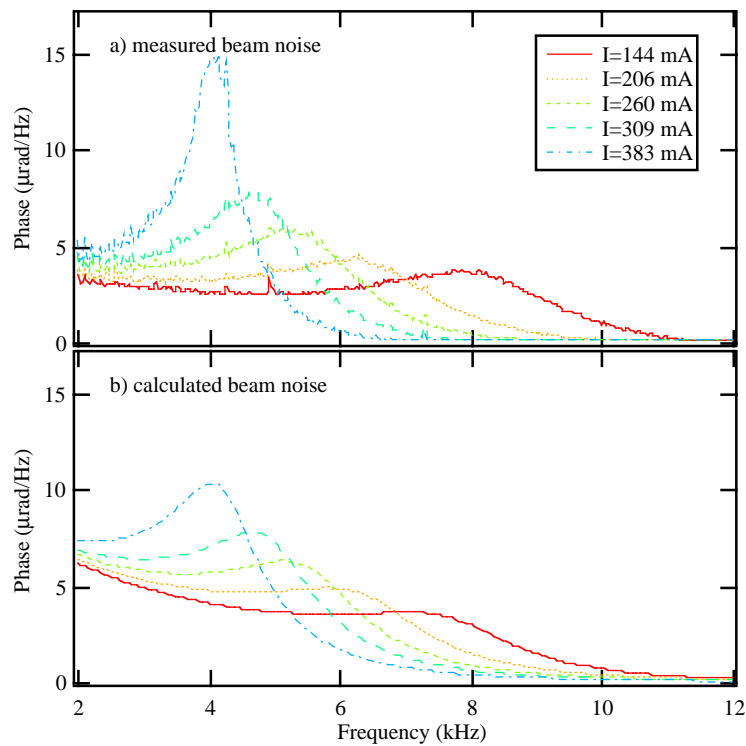


Figure 6. Measured and calculated spectrum of beam phase oscillations as a function of current.

To improve the situation at the ALS, we simply replaced the existing MO with a cleaner source. The result is shown in Figure 7: an overall improvement in the beam noise by a factor of six. This improvement was clearly visible on the infrared beamline. With the cleaner MO, harmonics of the klystron power supply are now visible in the beam spectrum. Improvements being planned include an additional phase feedback loop using a separate beam phase detector.

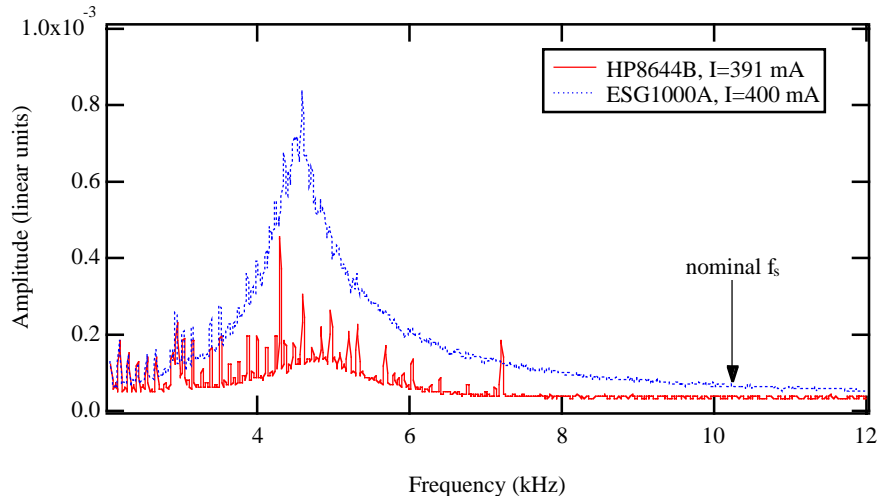


Figure 7. Comparison of beam motion for two MO sources.

Longitudinal Beam Dynamics at Injection

Reported by John Byrd and Stefano De Santis

Optimizing beam injection into electron rings is important for increasing the filling rate and reducing radiation background. Understanding the injection process has become increasingly important for the continuous-top-up injection that maintains a constant beam current. We have begun a study of beam dynamics at injection in the ALS with an initial emphasis on longitudinal beam dynamics. Some of the questions we hope to resolve include the following: What is the proper adjustment of the injected energy and phase for maximum capture in the storage ring? What are the loss mechanisms during injection? How do we minimally disturb the stored beam?

Some Possible Outcomes of Injection

Consider the injection of a bunch into a storage ring bucket as shown in Figure 8. If the bunch is injected away from the center of the bucket, either in phase or energy, as shown in Figure 8a, it will rotate in the bucket until it eventually damps to the stored beam. There may also be a mismatch of the injected bunch shape to the rf bucket, as shown in Figure 8 b, resulting in a quadrupole oscillation.

In these measurements we looked at the beam intensity following injection using a photomultiplier tube observing the intensity of synchrotron light. The photomultiplier is gated at the revolution frequency (1.5 MHz) synchronously with the passage of the injected bunch. It is then possible to have a measure of the bunch current from turn to turn proportional to the intensity of the synchrotron light emitted. Figure 9 shows a typical signal obtained injecting into an empty bucket; the time scale of the current decay is several milliseconds, indicating that the energy-phase acceptance is the limiting factor.

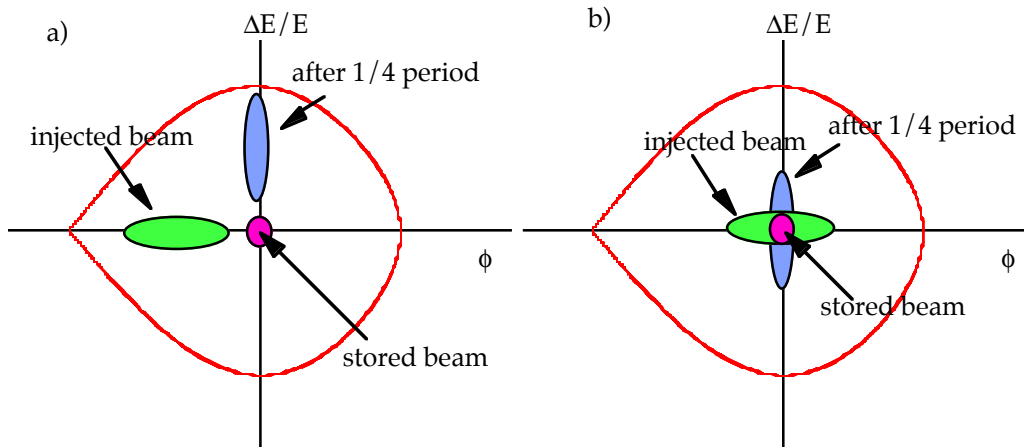


Figure 8. Beam phase space mismatch to the RF bucket at injection in two cases: (a) for phase offset and shape mismatch, resulting in dipole and quadrupole oscillations, and (b) for only a shape mismatch, resulting in quadrupole oscillations.

We can also look at the offset in the phase of the center-of-charge by detecting the phase of the signal induced in a beam position monitor. Shown in Figure 10 is an oscilloscope trace of this signal following injection with and without an energy offset to the injected beam.

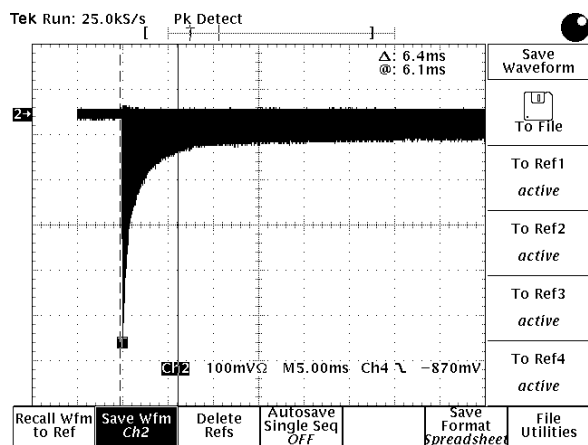


Figure 9. Photomultiplier tube data on BL 3.1, showing injection transient.

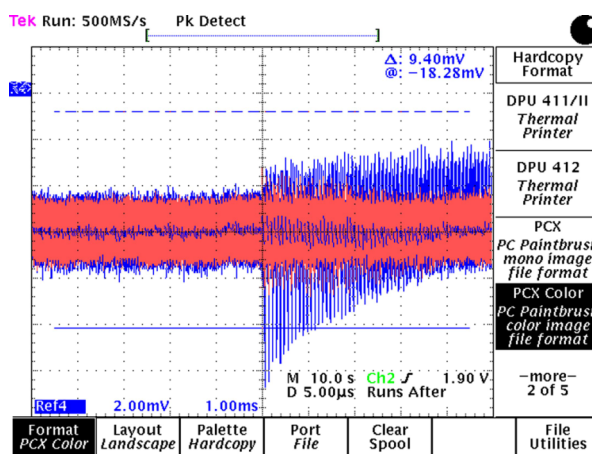


Figure 10. Longitudinal feedback pickups signal. Off-energy (dark) and on-energy (light) injection.

After increasing the energy of the injected beam by almost 1%, setting a new delay on the extraction trigger control, and re-tuning the transfer line from the booster to the storage ring, the injection rate went up from around 1 mA/shot to above 1.5 mA/shot.

We can make a detailed study of the longitudinal dynamics using a dual-scan synchroscan streak camera, with which we observe the time evolution of the longitudinal beam distribution following injection. When an electron bunch is injected into the storage ring, its length and energy spread will either grow or damp to the natural bunch length and energy spread of the storage ring; in the latter case the damping occurs over several radiation damping times. In the ALS, the injected bunch length is about five times the natural bunch length, and the injected energy spread is close to the natural energy spread. If this mismatched bunch is injected into the center of an rf bucket, it rotates in the bucket at the synchrotron frequency, modulating the bunch length as shown schematically in Figure 8b. However, the nonlinearity of the rf voltage creates a

dependence of synchrotron frequency on amplitude, causing the bunch head and tail to advance slower in phase than the center, resulting in filamentation of the bunch distribution.

Shown in Figure 11a is a synchroscan camera image of the beam 0.3 ms after injection into an empty storage ring. The vertical axis represents the longitudinal bunch length in units of time, and the horizontal axis is time. The bunch length is modulated at half the synchrotron period of $87 \mu\text{s}$ due to the rotation of the mismatched bunch shape as shown in Figure 8. Figure 11b shows the synchroscan camera image 2.4 msec later. The bunch filamentation is evidenced by the tails forming on the bunch distribution. This compares very well with a simulated synchroscan camera image as shown in Figure 11c, where each vertical slice is the projection of the phase space distribution.

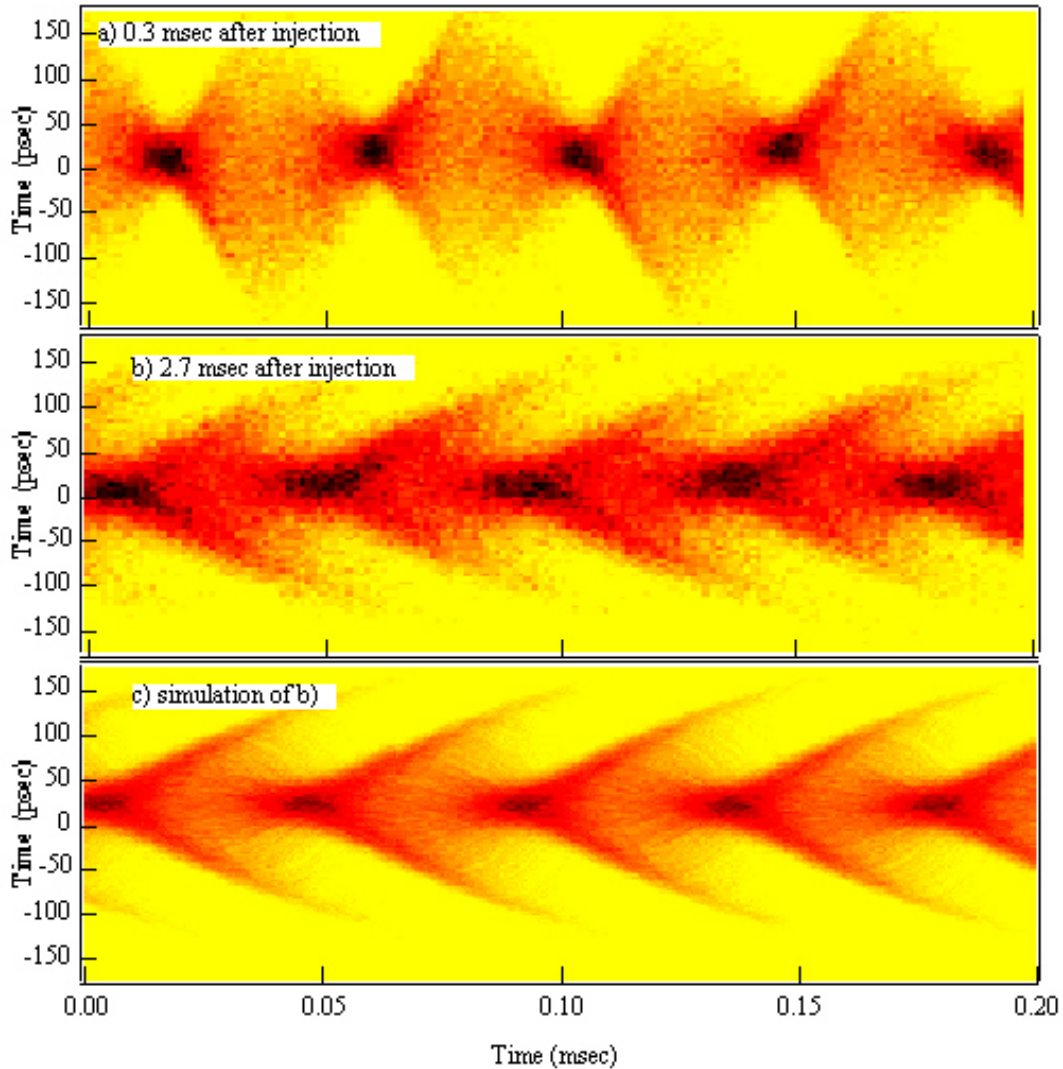


Figure 11. (a) Measured SC image 0.3 msec following injection showing modulation of the bunch length. (b) SC image 2.4 msec later showing filamentation of the large amplitude particles. (c) A computer simulated image found from tracking.

Lifetime and Momentum Acceptance

Reported by David Robin

Beam lifetime in a storage ring is limited by different effects: quantum lifetime, elastic gas scattering, inelastic gas scattering, and intrabeam scattering. The relative contributions of these various mechanisms have been measured for the ALS and are displayed in Table 3. As seen in the table, the lifetime limit is dominated by intrabeam (Touschek) scattering. In fact, Touschek scattering is the main lifetime limitation for most third-generation synchrotron radiation sources.

Table 3. Contributions of the lifetime limiting effects to the total lifetime at 400 mA in 1.5 GeV operation 1% emittance coupling.

	400 mA
quantum lifetime τ_q	>250 hours
elastic scattering lifetime τ_{el}	>18 hours
inelastic lifetime τ_{inel}	>55 hours
Touschek lifetime τ_{tou}	2.2 hours
total lifetime τ_t	>1.9 hours

Factors Affecting Touschek Lifetime

Touschek lifetime, τ_{tou} , is a function of the beam energy, E , the bunch current, I_b , the bunch volume, V_b , the bunch divergence, σ_x' , and the momentum acceptance, ϵ :

$$\frac{1}{\tau_{tou}(s)} \propto \frac{1}{E^3} \frac{I_b}{V_b(s)\sigma_x'(s)\epsilon(s)^2} f\left(\frac{\epsilon(s)^2}{\sigma_x'(s)E^2}\right)$$

The momentum acceptance, ϵ , is the maximum relative momentum deviation from the design momentum a particle can experience without being lost. τ_{tou} is strongly dependent upon the momentum acceptance (roughly proportional to the square of the momentum acceptance). The bunch volume, bunch divergence, and momentum acceptance all depend upon the longitudinal position, s , in the ring. Therefore, τ_{tou} needs to be averaged over s .

The momentum acceptance is limited by either the rf aperture or the dynamic aperture. The rf aperture is determined by the size of the rf bucket, which is proportional to the square root of the rf cavity voltage, and can be increased by adding rf power. The dynamic aperture limits the aperture through synchrotron coupling, which causes particles with large energy offsets to begin large transverse oscillations, resulting in the particle colliding with a transverse aperture in the ring. The momentum acceptance is determined by the smaller of the rf aperture or dynamic aperture. Both of these apertures are displayed in Figure 12.

In Figure 12 the blue lines represent the induced amplitudes—one for the arc section and the other for the straight section. In the straight section, where there is no dispersion, the induced transverse amplitude is nearly zero. In the arc section, with finite dispersion, the induced amplitude is much larger. The momentum acceptance is shown by the intersection of these blue lines with the aperture, and is limited by the dynamic aperture in the arc and the rf aperture in the straight.

Great effort is spent during the design of the storage rings to insure that the dynamic aperture is greater than the rf aperture and thus does not limit the momentum acceptance. In the past year we have made many measurements of the momentum acceptance and found that, in many cases, the dynamic aperture, not the rf, aperture limits the momentum acceptance.

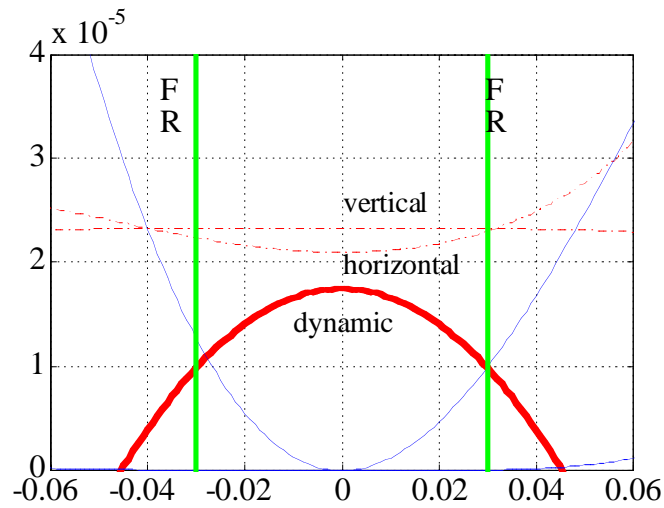


Figure 12. Contributions of the different aperture effects to the total momentum aperture. The thin lines are the invariant induced amplitudes at different positions in the ring.

Measurements of the Momentum Acceptance

We infer the acceptance primarily from measurements of the lifetime. Measurements of the lifetime as a function of the rf voltage were conducted under different storage ring conditions. The synchrotron tune was measured simultaneously, from which one can calculate the bunch length and the rf-bucket height. To enhance the effect of the Touschek scattering over other lifetime effects, a high current per bunch was filled in a few equidistant-spaced bunches. The low number of bunches avoids multibunch instabilities. The beam conditions were 1mA/bunch and 8 bunches (out of 328) filled. Results can be seen in Figure 13.

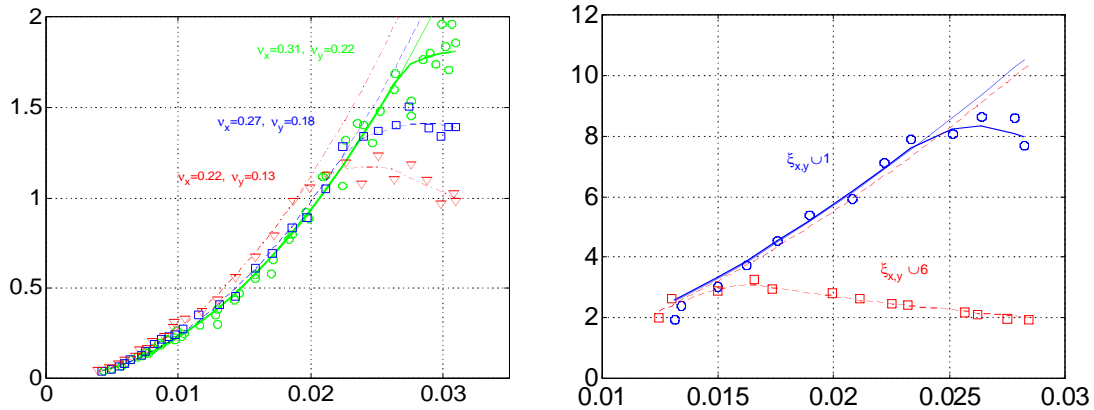


Figure 13. Beam lifetime as a function of the rf aperture with three different working points (left) and two different values of the chromaticities (right).

The data are fitted by applying the equation given earlier with the following fit parameters: assuming an initial 1% coupling the bunch volume is corrected by a constant factor that takes into account any volume changes such as variation of the coupling, instabilities, etc. The bunch volume is also adjusted according to the changing rf voltage (the bunch length is proportional to the inverse of the square root of the rf voltage). The other parameters are the momentum acceptances, ϵ , in the straight section and in the arc. Thus the data can be fitted with just three parameters.

The dynamic momentum aperture in the arcs can be seen in Figure 13 as the position where the data points start deviating from the quadratic line. In all cases this happens at values less than 3%. For the left plot, the dynamic momentum aperture of the arcs decreased as we moved to lower tunes. The aperture was measured to be 2.7% at the “high” tunes, 2.4% at the “middle” tunes, and 2.0% at the “low” tunes. In Figure 13 (*right*), we see that the dynamic momentum aperture decreased as we increased the chromaticity. When the horizontal and vertical chromaticities were adjusted to 6, the momentum acceptance in the arcs reduced to 1.4%.

Simulations of the Momentum Acceptance

Tracking calculations have been performed to understand the experimental results and test the accuracy of the model. Particles were tracked through the ALS lattice with a six-dimensional symplectic integrator. The following errors and constraints were included in the model to simulate the realistic machine:

- Physical aperture borders were included in the tracking to prevent particle oscillations outside the realistic vacuum chamber. This is important because large-amplitude particles may perform large, but stable, oscillations that would be outside the physical aperture but not lead to a loss of the particle in the tracking.
- Linear field errors are simulated according to the optics measurements done at the ALS with the response-matrix fitting method. These errors lead to a break in the lattice periodicity and excitation of resonances.
- Random skew quadrupole errors were distributed in all quadrupoles of the lattice and adjusted to obtain a 1% coupling.
- The wiggler was simulated as a chain of “hard-edged” bending magnets obtaining the correct linear focusing and longitudinal dynamics properties.

Particles were launched off-energy and off-axis with respect to their off-energy orbit and tracked for 512 turns or until lost. Results for three different tunes and three different chromaticities are shown in Figure 14. The thick symbols represent the measured momentum apertures, distributed along the curve showing the amplitude induced by Touschek scattering in the arc. In the case of the simulations, the aperture was calculated to be 2.8% at the “high” tunes, 2.4% at the “middle” tunes, and 1.9% at the “low” tunes. For the case of the chromaticity set to 6 the aperture was calculated to be 1.3%. The agreement between measurement and tracking is excellent.

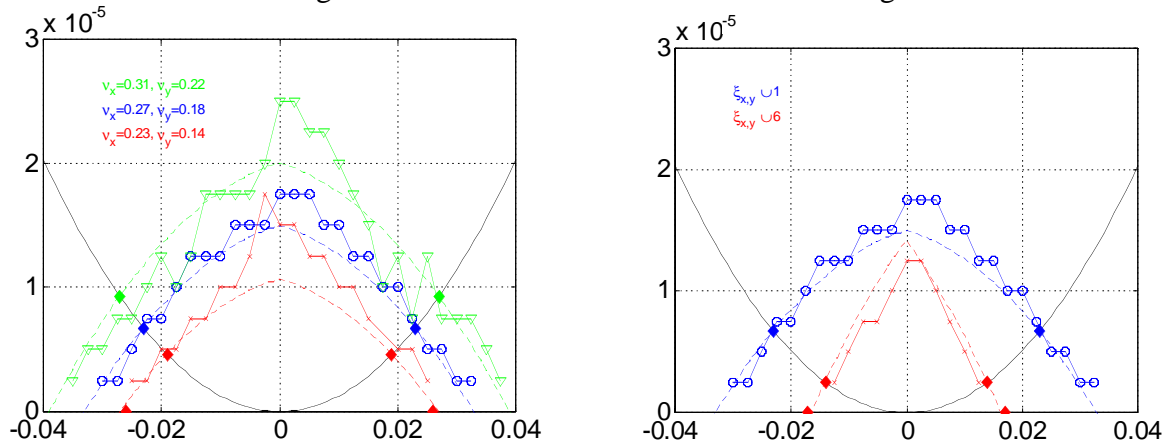


Figure 14. Maximum stable transverse emittance as a function of momentum deviation. The left side is a case with three different working points, while the right side shows two different chromaticities.

In addition to these measurements, the momentum acceptance was measured under various different conditions, including high coupling and with the wiggler magnet turned on. The results of all measurements are summarized in Table 4. The agreement between simulation and measurement is better than 15%.

Table 4. Measured and calculated momentum aperture in the straight and in the arc section for different machine conditions.

Coupling	Chromaticity	Horizontal Tune	Vertical Tune	Measured ϵ (straight)	Measured ϵ (arc)	Calculated ϵ (straight)	Calculated ϵ (arc)
Wiggler off							
0.01	1.0	0.31	0.22	>3.2%	2.7%	3.9%	2.8%
0.01	1.0	0.27	0.18	>3.3%	2.4%	3.3%	2.4%
0.01	1.0	0.22	0.13	2.6%	2.0%	2.8%	1.9%
0.01	1.0	0.27	0.18	>2.8%	2.8%	-	-
0.01	6.0	0.27	0.18	1.7%	1.4%	1.6%	1.3%
0.10	1.0	0.27	0.18	2.8%	2.3%	3.0%	1.8%
Wiggler on							
0.01	1.0	0.27	0.18	>3.3%	2.1%	3.0%	2.1%
0.10	1.0	0.27	0.18	>2.8%	1.6%	2.8%	1.6%
0.10	0.0	0.27	0.18	>2.8%	1.7%	-	-
0.10	6.0	0.27	0.18	1.8%	1.3%	-	-
0.10	1.0	0.31	0.22	>3.2%	1.9%	3.5%	2.0%

At this time we feel that we can draw several conclusions:

- The dynamic aperture limits the momentum acceptance in the ALS.
- Particles tend to get lost when they collide with the narrow vertical aperture in the ring. The mechanism for particle loss appears to be nonlinear synchrotron coupling that causes the motion of particles to reach the vertical aperture.
- By knowing the location of these dangerous synchrotron resonances, as well as the knowledge of the tune shifts with energy and with amplitude, one can accurately estimate the aperture.

Understanding these dynamic limits is important in order to improve the lifetime in the ALS and accurately predict the lifetime (and dynamic aperture) in future machines.

Orbit Compensation of the Elliptically Polarized Undulator (EPU)

Reported by Greg Portmann

By changing the insertion device gap, the photon beam energy can be varied. Unfortunately, the electron beam orbit is perturbed when the gap is changed. However, the resulting orbit perturbation can be removed by adjusting the corrector magnets on either side of the insertion device. Without compensation, the electron beam would move by 200 to 400 microns (depending on the device) during a full open-to-closed transition of the gap. Using a simple feedforward lookup table, the orbit accuracy can be maintained to ± 10 microns. Due to the effectiveness of the feedforward system, ALS users can freely adjust the gaps at any time.

The elliptically polarized undulator (EPU) adds a new dimension to the problem. The EPU has not only a vertical gap drive system, but a longitudinal drive as well. The vertical gap is varied to control the energy of the radiation. At a given vertical gap, the longitudinal gap is changed in

order to control the helicity of the radiation. Unfortunately, this motion produces gap-dependent error fields. We have shown that, despite this added degree of complexity, we can compensate for these error fields using lookup tables, just as is done with the less complicated insertion devices. Figure 15 shows the vertical feedforward. A one gauss-centimeter dipole error will cause a 1–1.5 micron distortion in the storage ring orbit.

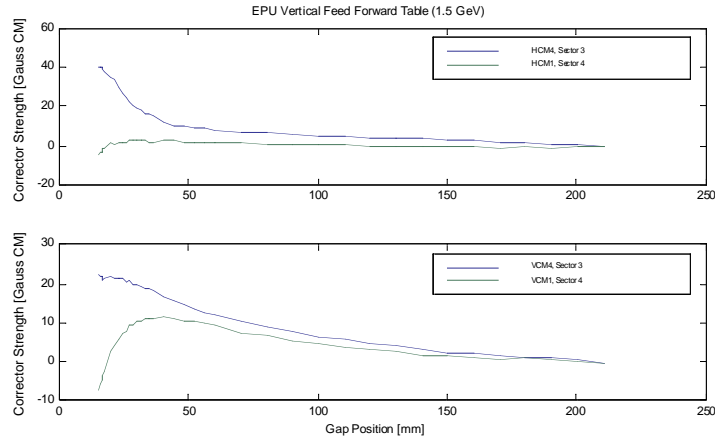


Figure 15. Vertical feedforward table for the EPU.

If the longitudinal motion of the EPU were left uncompensated, the maximum orbit distortion would be ± 50 microns horizontally and ± 200 microns vertically. Figures 16 and 17 show the 2-dimensional feedforward tables for each plane. It takes about 2 hours of machine time to generate a 2-dimensional table, compared to 10 minutes for the 1-dimensional vertical table. The sensitivity of these tables to the electron beam position in the insertion device is quite small: 10–20 microns over 1 mm of orbit change through the insertion device. Since the electron beam orbit should be stable to 0.05 mm or less, the 2-dimensional table should not need to be generated very often.

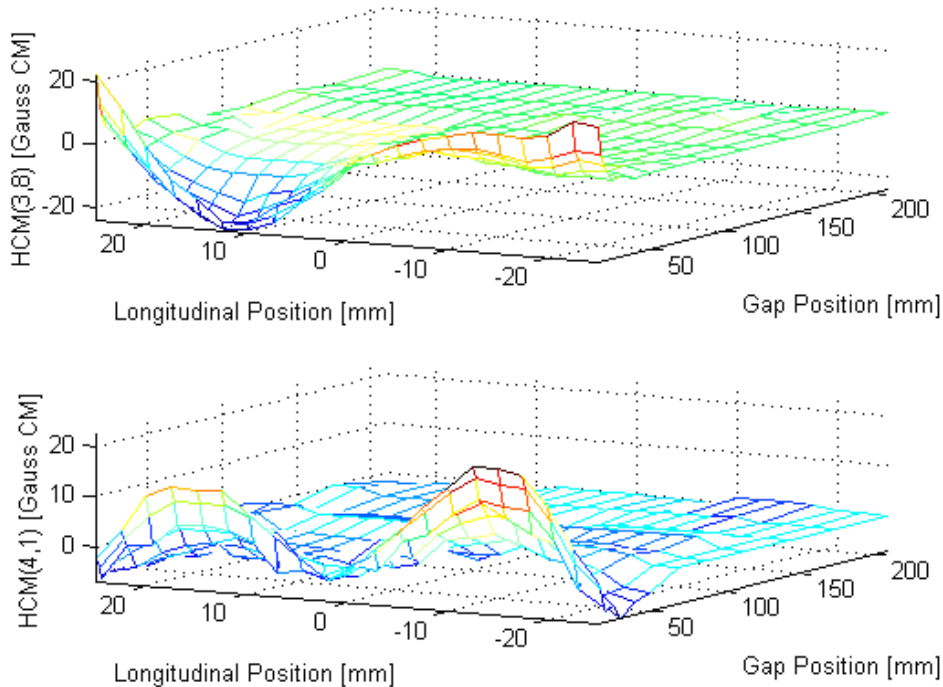


Figure 16. Longitudinal feedforward table in the horizontal orbit direction.

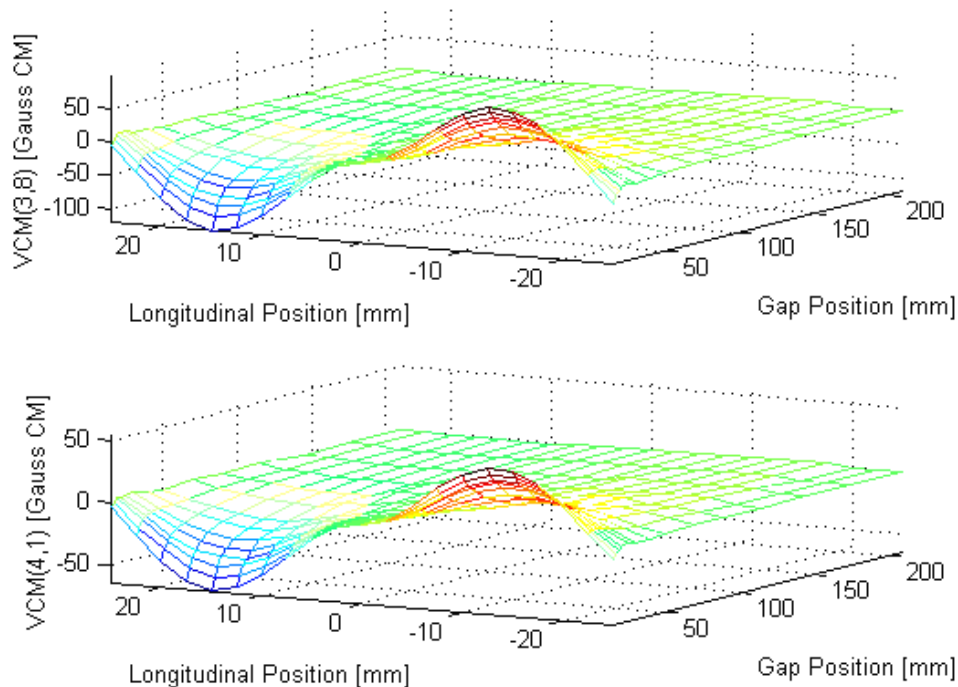


Figure 17. Longitudinal feed forward table in the vertical orbit direction.

Increasing Beam Lifetime Without Losing Brightness

Reported by John Byrd

The beam lifetime is one of the most important parameters to the ALS users. As described earlier in this chapter, it is dominated by large-angle intrabeam (Touschek) scattering, which occurs when electrons within the bunch scatter and transfer enough momentum that they are knocked outside the momentum acceptance of the storage ring. For a given beam energy, we can improve the lifetime by either increasing the momentum acceptance of the ring or by reducing the charge density of the electron bunch. We expect only marginal improvements in the momentum acceptance as either the rf voltage is slowly increased or as the momentum acceptance of the lattice is better understood.

A Lifetime Improvement Idea

We currently increase the lifetime by increasing the vertical beam size through excitation of the betatron coupling resonance, effectively reducing the transverse beam brightness. An alternative has been proposed where the bunch is lengthened using a third-harmonic voltage of the 500 MHz main accelerating cavities as illustrated in Figure 18.

The harmonic voltage is adjusted to cancel the slope of the main rf voltage at the bunch center, effectively lengthening the bunch. The effect on the bunch shape at optimum lengthening is shown in Figure 19. We expect an increase of lifetime of a factor of 3 at optimum.

To produce the required harmonic voltage, a team of LBNL physicists and engineers have designed a 1.5 GHz (3 x 500 MHz) rf cavity to be installed at the ALS. The cavities (Figure 20) were fabricated at Lawrence Livermore National Laboratory by the same team that made the main rf cavities for the PEP-II B Factory. Five such cavities will be installed in the downstream half of straight section 2 in June 1999. The cavities will be operated in a passive mode, i.e., the cavity voltage will be generated by the beam. The design is upgradeable to an active system, should the need arise.

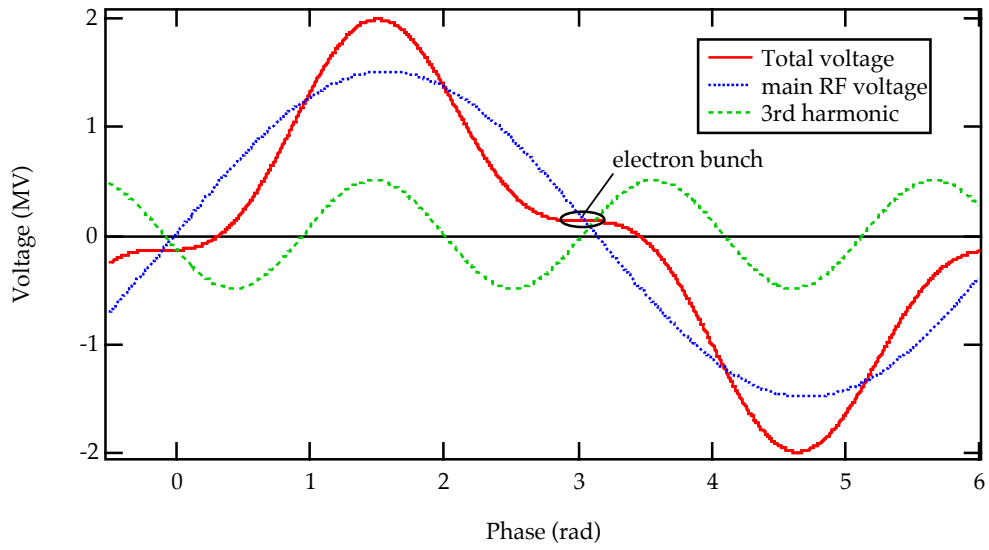


Figure 18. Third-harmonic bunch lengthening scheme.

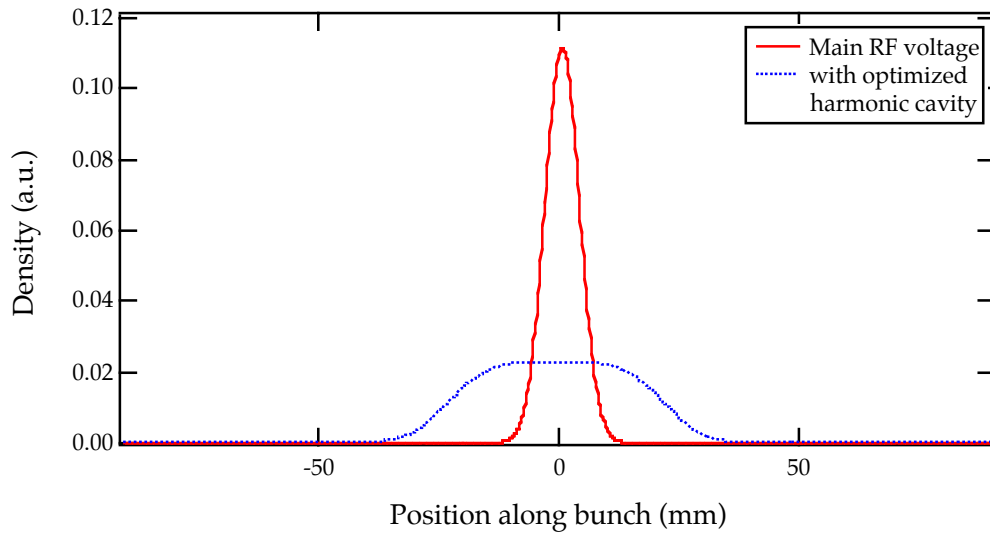


Figure 19. Effect of third-harmonic cavity upon bunch shape, at optimum lengthening.

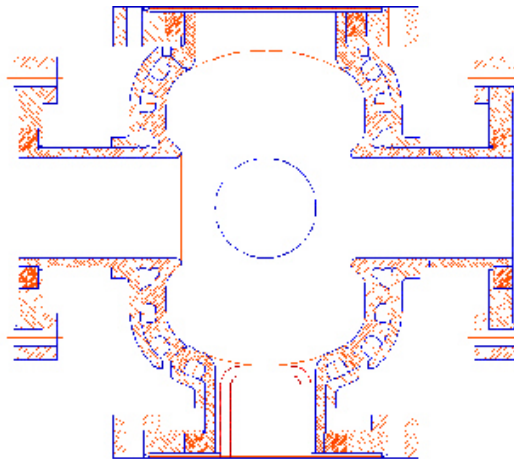


Figure 20. Third-harmonic cavity (1.5 GHz).

Superbends at the ALS

Reported by David Robin

There is an increasing demand for more high-energy, high-brightness x-ray ports at the Advanced Light Source (ALS). To satisfy this demand, a plan is being implemented to replace three 1.3-T normal-conducting bend magnets with three 5-T superconducting bend magnets. In principle, one could create high-energy sources by placing wigglers or wavelength shifters in the long straight sections. However, of the 12 straight sections, only 2.5 are empty at present. By replacing the existing bends with high-field bends, we can obtain additional high-energy sources without using the straight sections. Figure 21 compares the flux and brightness of the superbends with other sources of high-energy photons. Compared to a normal ALS bend, a superbend provides an order of magnitude more flux and brightness at 10 keV—two orders of magnitude at 20 keV.

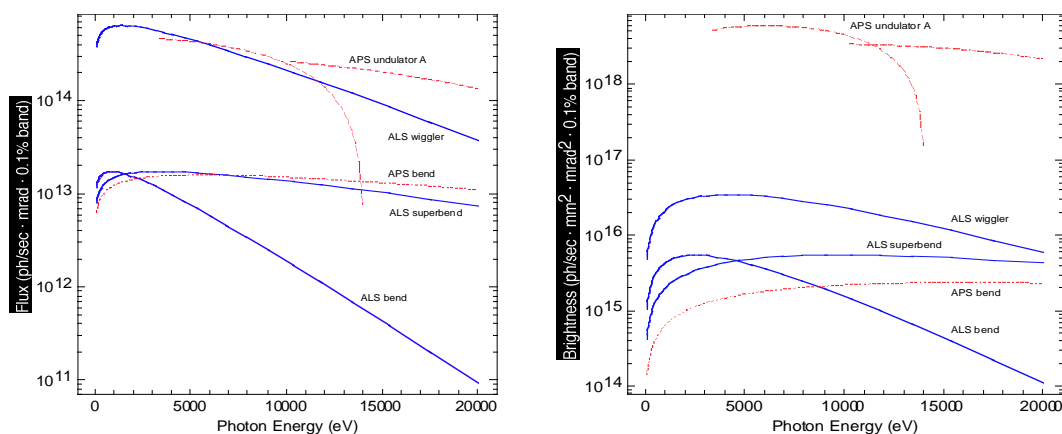


Figure 21. The flux (*left*) and brightness (*right*) of several high energy sources: the normal ALS bend, a superbend, the W16 wiggler, and APS bend and APS undulator A.

Planned Configuration with Superbends

The plan is to modify three of the twelve ALS sectors to include superbends. A typical sector can be seen in Figure 22 (top). The sector has three dipole magnets, each bending the beam by 10°. The dipoles are combined function magnets having both dipole and quadrupole field components. The superbends, unlike the normal dipoles, do not have a large quadrupole (focusing component); therefore additional quadrupoles are placed on both sides. Figure 22 shows the lattice of a sector in its original configuration (upper) and as modified to include a superbend and two additional quadrupoles.

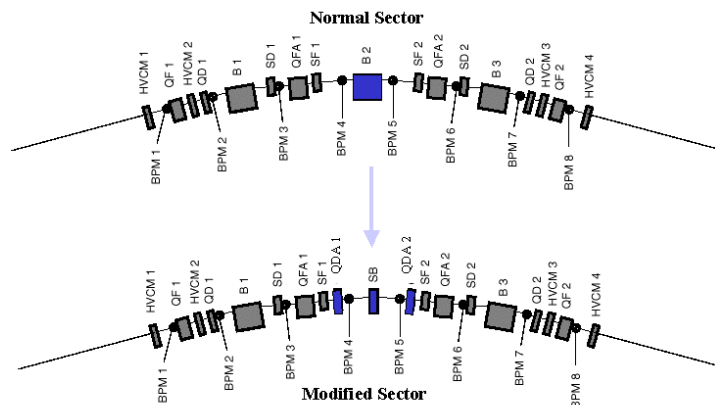


Figure 22. Magnet layout of a normal (*top*) and modified (*bottom*) sector.

In Table 5, the parameters of the ALS are given without the superbends and matched to zero dispersion in the straights (column 1); with 3 superbends and matched to zero dispersion in the straights (column 2); and finally with 3 superbends matched to 6 cm dispersion

in the straights (column 3). Due to increased quantum fluctuation with the superbends, the horizontal emittance, ϵ_x , increases. However, by operating with finite dispersion in the straight section, it is possible to reduce ϵ_x .

Table 5. Storage ring parameters without superbends, with three ($\eta_x=0$), and with three ($\eta_x=6\text{cm}$).

	No Superbends ($\eta_x = 0$)	Three Superbends ($\eta_x = 0$)	Three Superbends ($\eta_x = 6 \text{ cm}$)
Energy	1.9 GeV	1.9 GeV	1.9 GeV
ϵ_x	5.5 [nm rad]	13 [nm rad]	7.5 [nm rad]
σ_E	0.08%	0.10%	0.10%
$\Delta E/\text{turn}$	232 keV	281 keV	281 keV

Impact on Machine Performance

It is important that there be no major impact on normal operation; therefore it is necessary to check that the stability of the beam motion remains sufficient for good injection and lifetime. We know that the superbends will perturb the ring's 12-fold periodicity, as well as introducing some nonlinear fields, which may excite low-order resonances that affect the beam dynamics.

A useful way to visualize the impact of periodicity breaking is through tune scans. We use simple 4x4 matrix code to do the tracking where the sextupoles are modeled as thin kicks. The superbends are modeled as isomagnetic sector bends with linear hard-edged fringe fields. The strength of the magnetic field, B , and length, L , is adjusted such that the longitudinal integral of B and B^2 is the same as for the true superbend fields. The chromaticity is set to zero in both planes and the dispersion fitted to zero in the straight sections. Attached to the tracking code is a frequency analysis post processor that numerically computes the fundamental frequencies of an orbit.

First the betatron tunes are set. Then a particle is launched with an initial offset of 10 mm horizontally and 1 mm vertically and tracked for 1024 turns or until lost. If the particle survives 1024 turns, the frequency post processor computes the fundamental frequencies for that particle. The procedure is then repeated for many different tunes. In total the machine is adjusted to 900 tunes (on an evenly spaced grid of 31x31 tunes between $\nu_x = 14.1$ to 14.4 and $\nu_y = 8.1$ to 8.4). The results are plotted in Figure 23.

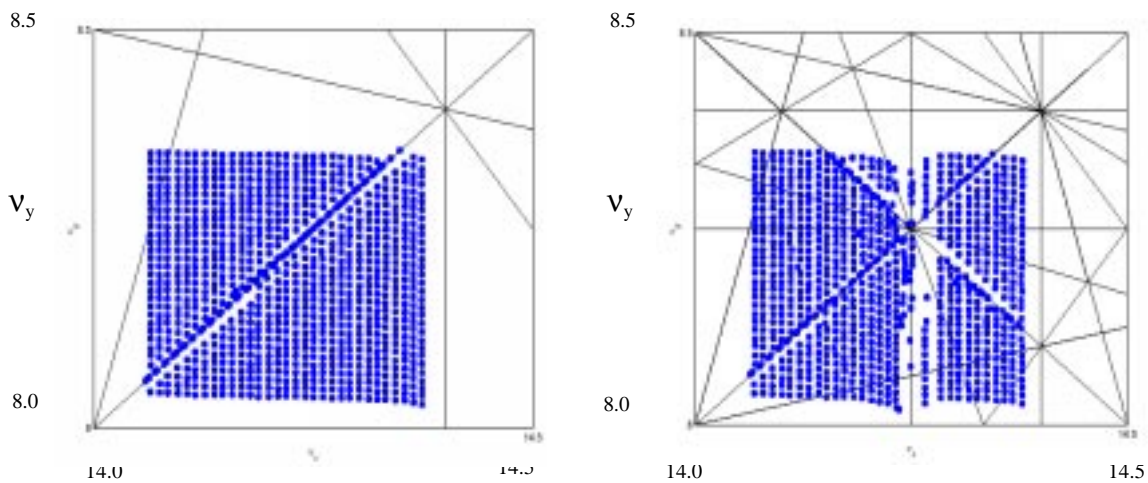


Figure 23. Tunescans: A comparison of 0 and 3 superbends.

On the left in Figure 23 is the lattice with no superbends. On the right is a lattice with three superbends, evenly spaced. Superimposed lines plot all allowed resonances of up to the 5th order. The dots correspond to the numerically calculated frequencies. Excitation of resonances can be observed either from missing points or distortion in the point spacing.

In the case of no superbends (*left*), one only sees the influence of the $2\nu_x - 2\nu_y = 12$ resonance. In the case of three evenly spaced superbends (*right*), one sees that there are more resonances excited. In particular, one sees a 4th-order resonance, $4\nu_x = 57$, that is strongly excited and also several coupled resonances that cross at $\nu_x = 14.25$ and $\nu_y = 8.25$. In these regions, the motion of large-amplitude particles is chaotic. However, there still seem to be large regions in tune space where it is possible to operate. This is not true in the case of three superbends located asymmetrically around the ring. In that case, the tunes scans were greatly distorted, with many missing points. Based upon the tunes scans for the three evenly spaced superbends, a working point was chosen ($\nu_x = 14.25$ and $\nu_y = 8.2$) for more detailed tracking studies.

For more quantitative particle tracking studies, we use a 6-D symplectic integrator. We include a ± 25 mm horizontal and ± 4 mm vertical physical aperture. Quadrupole gradient errors are included that match the existing machine producing a 5% horizontal and vertical β -beat and 1% coupling. For the superbends we included an integrated sextupole (-5.6 m^{-2}) and decapole (-4.1 m^{-4}), which are the values measured for a prototype magnet.⁴

At the ALS, injection is done off axis in the horizontal plane. It is necessary to have at least a 7-mm horizontal aperture to capture the beam. So for injection studies, the particles were launched with different horizontal offsets and no energy offset and tracked for 512 turns or until lost. The results can be seen in Figure 24. Without superbends, the smallest aperture with errors was calculated to be 14 mm. With superbends, it reduced to 11 mm, but there still exists a sufficiently large region for injection.

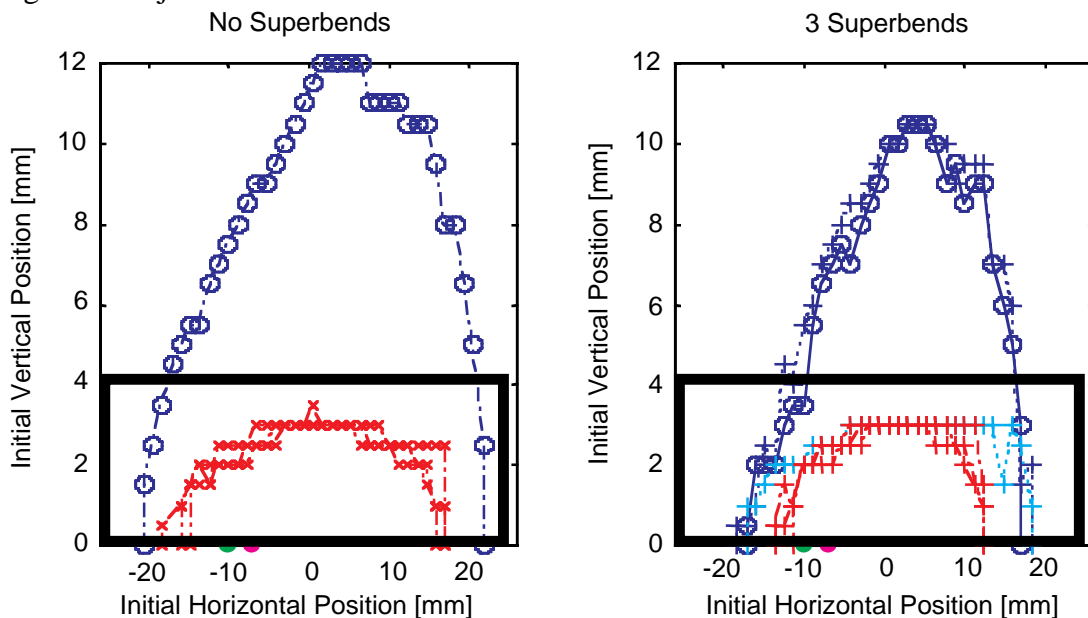


Figure 24. Injection simulations for a lattice without superbends (left) and one with superbends (right). The blue circles are the results with no errors and no physical aperture. The red crosses are the results with field errors and realistic physical apertures.

⁴ C. E. Taylor et al., "Test of a High-Field Bend Magnet for the ALS," *Proceedings of the 1998 Applied Superconductivity Conference*.

As previously mentioned, the lifetime is determined by intrabeam scattering. Therefore it is important to ensure that the momentum acceptance is acceptably large. At the ALS, the dynamic momentum acceptance is smallest in the arcs and largest in the straight section. We were particularly concerned that a reduction in the momentum acceptance in the arcs would make it less than the rf acceptance and reduce the lifetime. To determine the dynamic momentum acceptance, the particles are launched with an initial horizontal offset and an energy offset and tracked with synchrotron oscillations.

The results of the tracking that can be seen in Figure 25 showed that the dynamic momentum acceptance (in the arcs) decreased from 2.8% to 2.4% with superbends. However, this is still larger than the rf acceptance, which is 2% at 1.9 GeV. Therefore there should be no impact on the lifetime.

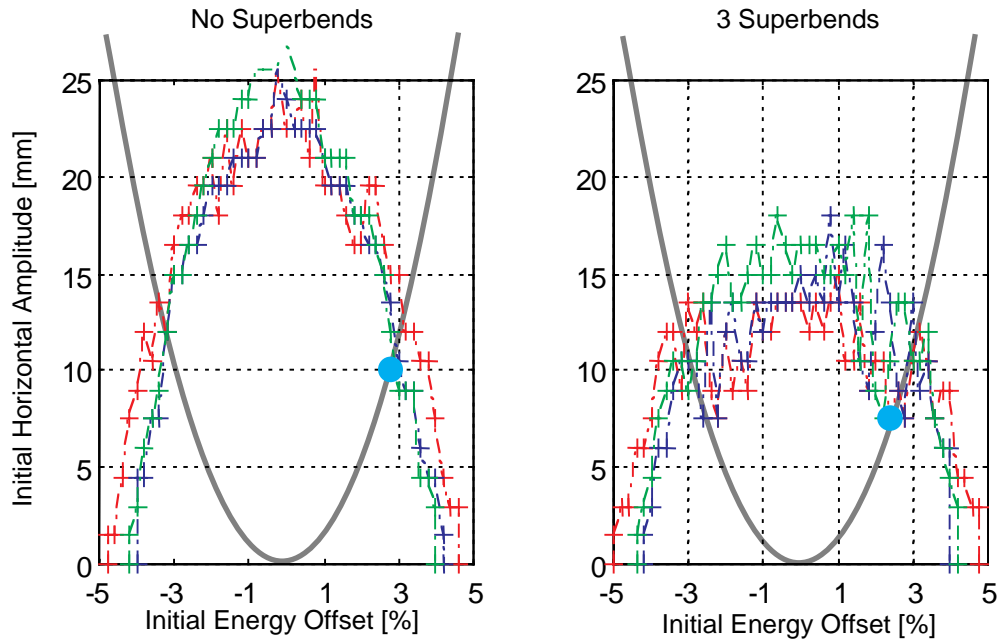


Figure 25. Off energy tracking with no superbends (*left*) and 3 superbends (*right*). Three error seeds are presented. The black line shows the induced betatron amplitude in the arcs. The momentum acceptance (marked with a blue dot) is given by the intersection of the tracking data with the induced amplitude.

If all goes as planned, the ALS will be operating successfully with 3 superbends in 2001.